2019

Reversible Mechanical Deformations of Soft Microchannel Networks for Sensing in Soft Robotic Systems

Abhiteja Konda
Argonne National Laboratory Lemont & University of Nebraska–Lincoln

Donghee Lee
University of Nebraska Medical Center & University of Nebraska–Lincoln

Taesun You
Houston District Texas Department of Transportation

Xiaoyan Wang
University of Nebraska Medical Center

Sangjin Ryu
University of Nebraska-Lincoln, sangjin.ryu@unl.edu

See next page for additional authors

ADVANCED INTELLIGENT SYSTEMS
Open Access
www.advintellsyst.com

Reversible Mechanical Deformations of Soft Microchannel Networks for Sensing in Soft Robotic Systems

Abhiteja Konda, Donghee Lee, Taesun You, Xiaoyan Wang, Sangjin Ryu, and Stephen A. Morin**

Microfluidics has enabled numerous applications in, for example, analytical chemistry, medical diagnostics, microelectronics, and soft robotics. In most of these applications, the geometries of the microchannels are of fixed dimensions that (ideally) remain invariant during operation. In soft robotics, however, the geometries of the microchannels contained in soft actuation systems are inherently dynamic, and the specific dimensions are expected to change during operation, and, by extension, the fluid transport properties of the system are variable. If this characteristic is not properly considered, or if methods are not developed to control it, the progress of soft robotic devices with distributed fluid transport systems can be hampered. Herein, the deformation of soft microchannel networks is investigated using a finite-element method and experimental observations, and the understandings are applied to imbibe sensing capabilities in soft robots that have integrated microfluidic networks with dynamic channel geometries of predictable dimensions. This approach enables the fabrication of soft fluid transport systems with deterministic deformation characteristics—a capability that is specifically applied to touch and actuation sensing in soft actuators. This work provides insight into the channel deformation processes expected in soft robotic systems with embedded networks of microchannels, enabling devices with reliable/predictable transport properties.

The application of microfluidics in several fields, including soft robotics,[1] medical diagnostics,[2] and chemical and biological sciences,[3] has led to increased interest in devices with intricate geometries and multifunctional capabilities. Most applications incorporate channel networks with fixed dimensions that remain invariant during their operations;[4] however, in flexible, stretchable systems, such as in soft robotics (e.g., fluid elastomeric actuators [FEAs]), the microchannel networks undergo deformation during actuation.[1a,5] While the mechanism of channel deformation has been extensively studied,[6] its effect on soft microfluidic systems is relatively unexplored, and sensing deformations in these systems has proved particularly challenging. A popular approach involves filling microchannel networks with liquid metals to generate conductive, deformable traces. Monitoring changes to the electrical properties (e.g., resistivity and capacitance) during deformation provides a convenient means of sensing motion;[7] however, these filled microchannels are typically close-ended, serving no

Dr. A. Konda, Prof. S. A. Morin
Department of Chemistry
University of Nebraska–Lincoln
Lincoln, NE 68588, USA
E-mail: smorin2@unl.edu

Dr. A. Konda
Nanoscience and Technology Division
Argonne National Laboratory
Lemont, IL 60439, USA

Dr. D. Lee, Prof. S. Ryu
Department of Mechanical and Materials Engineering
University of Nebraska–Lincoln
Nebraska Hall, Lincoln, NE 68588, USA
E-mail: sangjin.ryu@unl.edu

The ORCID identification number(s) for the author(s) of this article can be found under https://doi.org/10.1002/aisy.201900027.

DOI: 10.1002/aisy.201900027

Dr. D. Lee
Department of Genetics, Cell Biology and Anatomy
University of Nebraska Medical Center
Durham Research Center II
Omaha, NE 68106, USA

Dr. T. You
Houston District
Texas Department of Transportation
Houston, TX 77007, USA

X. Wang
Department of Pharmaceutical Sciences
University of Nebraska Medical Center College of Pharmacy
Omaha, NE 68198, USA

Prof. S. Ryu, Prof. S. A. Morin
Nebraska Center for Materials and Nanoscience
University of Nebraska–Lincoln
Lincoln, NE 68588, USA

transport function. So-called "piezoresistive" strain sensors (e.g., those fabricated from elastomers doped with carbon black or from conductive inks) have also been used as motion sensors in soft actuators, but again these systems are independent and serve no ulterior function.[8]

We developed a method that allowed us to predict the cross-sectional (CS) geometry of microchannels at well-defined states of compression, experimentally verified these findings, and used it to imbibe sensing capability in soft actuators. In particular, we used a finite-element method (FEM) and the mechanical properties of the elastomeric polymer (polydimethylsiloxane [PDMS]) to predict the morphology and dimensions of soft microchannels under compression and compared them with experimental results obtained using a range of characterization techniques (e.g., optical microscopy and micro-computed tomography [micro-CT]). We also demonstrated the ability to measure the flow parameters (e.g., volume flow rate) in both static systems (those seen in traditional microfluidics) and dynamic systems (e.g., those seen in soft robotics) where the microchannels are deformed during actuation. We applied this understanding to integrate touch- or bend-sensing capabilities in soft robots, where the change in the volume flow rate was correlated with the state of actuation—this strategy represents an important opportunity in collocated functionality.

In soft robotics, predicting the fluid transport properties of microchannels during deformation could lead to soft systems with purpose-built, distributed transport systems required for actuation and on-board chemical/physical functions (e.g., analysis, sensing, and detection).[1b,9] Beyond soft robotics, understanding the deformation mechanics and the ability to predict its effect on channel morphologies and dimensions could be useful to a range of other capabilities, including 1) the generation of intricate channel geometries that are, otherwise, challenging to fabricate using replica molding alone;[10] 2) the selective separation of different sized particles using dynamic channel cross sections in microfluidics;[10c] and 3) the study of molecular transport[11] for mixing fluids[12] or for mimicking biological environments (e.g., circulatory systems).[13]

Soft robotics, as a field, has emerged from simple FEAs that use actuation for manipulation and locomotion,[1a,14] to sophisticated systems with integrated sensors.[7c,e,f,15] Pneumatics is commonly used for the actuation of soft robots. While early demonstrations used external pumps to generate pneumatic power,[1a,5] recent work used on-board chemical reactions for the generation of pneumatic pressure, thus leading to autonomous multifunctional soft robots.[1b,9a] It is clear that the design and fabrication of self-powered soft robots or soft robots with advanced capabilities (e.g., onboard analytics) will require integrated microchannel networks for transporting different fluids.[14] These fluids (e.g., gases) can be used for actuation[1a,14,15] or for advanced functions, such as supplying power (e.g., via chemical fuels),[1b,9a] or onboard detection and/or analysis using liquid metals or reagents.[16] While existing methods (e.g., those that involve liquid metals) are sensitive with rapid response times, they involve the use of dedicated electrical instruments and costly materials (e.g., eutectic indium–gallium). The presented approach is relatively simple: changes in the fluid transport properties of microfluidic fuel/reagent delivery systems can be correlated with touch and actuation sensing, and, because these fuels/reagents will be a prerequisite to various autonomous functions, this capability can be achieved without requiring extra equipment or dedicated systems to process signals. The fluid transport systems will satisfy sensing and operation maintenance functions, simultaneously.

Although deformation of nano/microchannels has been studied previously,[6c,17] and used to create nanofluidic systems[6a,b] and nanoscale patterns,[18] it has not been explored in relation to soft robotics for the control/prediction of fluid transport properties. FEM simulation has been widely used for modeling the deformation of PDMS under mechanical stress.[19] While linear elastic models can be used to predict the behavior of PDMS at small deformations (within the linear elasticity region),[20] hyperelastic models are often used to predict relatively larger deformations, such as those common in soft robotics.[21] Some of the popular hyperelastic models include the second-order Ogden model,[22] the polynomial model,[23] the Yeoh model,[24] and the Mooney–Rivlin model.[23,25] In our previous work, we demonstrated the ability to modulate the channel CS morphology and used it to redirect fluid flow within the reactor and to control the degree of mixing.[26] Herein, we modeled, designed, and fabricated microfluidic systems, which, when exposed to different compressive stresses, changed the channel geometry predictably and, by extension, the fluid transport behavior (used to collocate touch or bend sensing).

We used 3D printing to fabricate the masters that were used in conjunction with traditional soft lithography to create microfluidic channel networks and FEAs. The 3D printing enabled rapid designing and prototyping of the desired microfluidic and actuation devices.[26,27] We used elastomeric polymers common to soft robotics:[28] the devices used for systematic studies of the mechanical deformation were fabricated in PDMS (**Figure 1**a,b), and the soft robotic actuators were fabricated using a combination of Ecoflex 00-30 and 00-50. In addition to the suitable mechanical properties of these polymers for soft robotics,[28] they are available in a diversity of chemical formulations, which offer a wide range of stiffnesses.

As we used a long channel (36 mm) with a small cross section (1.5×1.5 mm^2), the strain along the long axis of the channel was negligible—strain due to the change of the channel length and the shear strains (γ_{xz} and γ_{yz}) are close to zero when the channel length (L) is much longer than the characteristic dimension (D) of channel cross section ($L/D >> 1$).[29] We, therefore, generated a 2D model consisting of plane strain quadrilateral elements to computationally predict channel cross section under compression (Figure 1c,d). We used experimentally measured stress–strain curves and the second-order Ogden hyperelastic model (which has been used to describe deformation of PDMS) to assign the material property of the PDMS (Figure S1, Supporting Information).[21a] We used different characterization techniques to observe the change in CS morphology and dimensions, including the analysis of replicates cast within the channels at different states of strain. In brief, epoxy resins were introduced into the deformed channels in a liquid state, allowed to solidify, and then cross-sectioned and characterized using optical microscopy or micro-CT (see Supporting Information). Optical microscopy was used to analyze the channel cross sections (both qualitatively and quantitatively, Figure 1f);

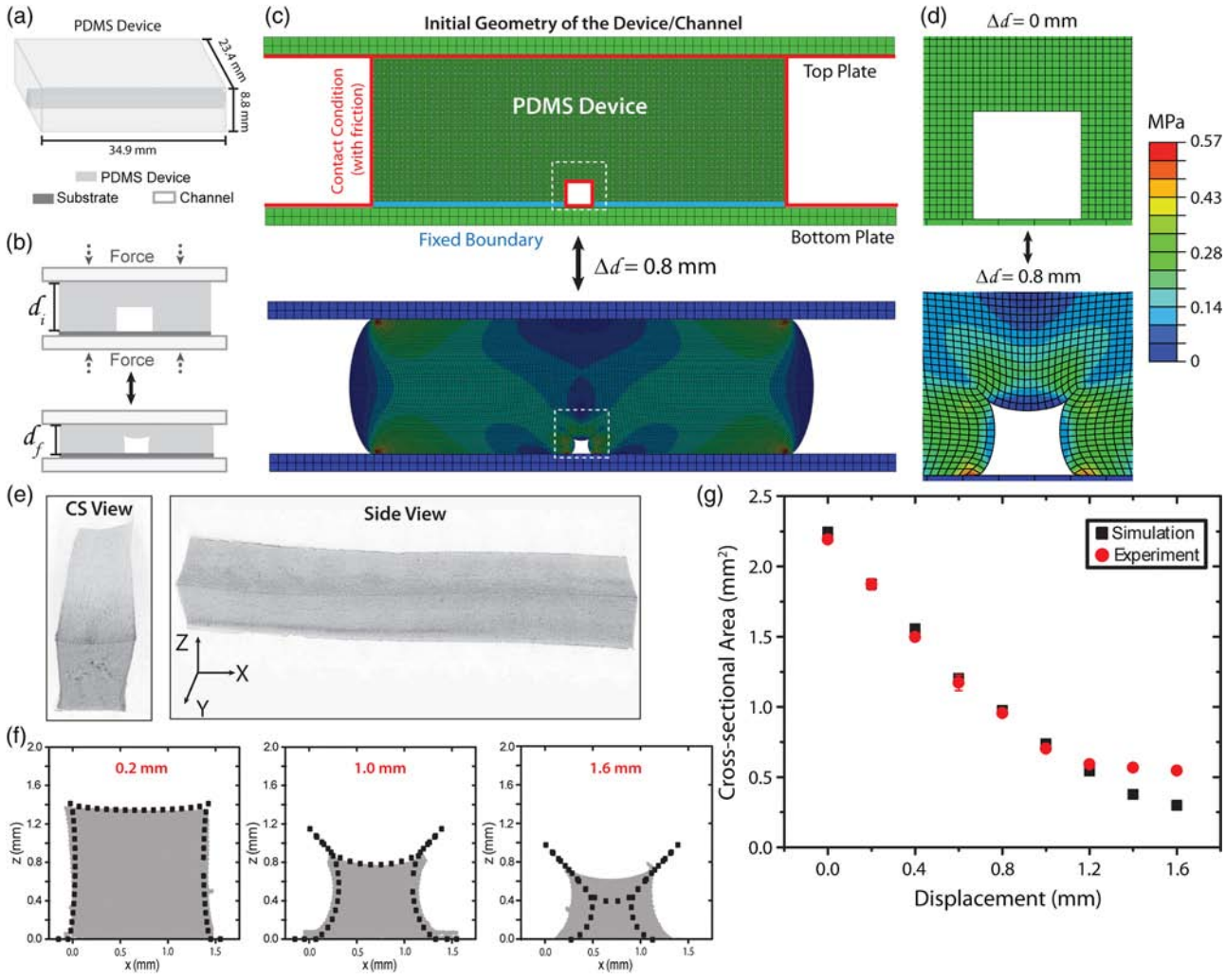

Figure 1. Comparison of simulated and experimental microchannel deformation. a,b) Schematic showing the a) device dimensions and b) experimental design for compression of microchannels. c,d) Illustration showing the boundary conditions for simulation using the FEM at 0 and 0.8 mm displacement. e) Micro-CT profile of an epoxy replicate for a 1.5 mm × 1.5 mm rectangular channel generated at a Δd value of 0.8 mm. f) Comparison of the simulated and experimentally observed channel morphologies for three Δd values. g) Plot comparing the calculated (using FEM simulation) and measured (using optical micrographs) CS area for the channel profiles at Δd values between 0.0 and 1.6 mm.

micro-CT was used to analyze the profile of entire channel (Figure 1e). We also observed the channel deformation mechanics in real time using a custom material testing system equipped with a high-resolution optical microscope (Figure S2, Supporting Information), which was useful in defining the boundary conditions for the FEM simulation (see Supporting Information and Video S1).

We studied the flow properties within the attached microchannels of an FEA during actuation (and associated deformation). In particular, we focused on the flow of liquids (e.g., water, which has a viscosity similar to many chemical/analytical reagents, fuels, etc.) as they are critical to the development of systems with predictable transport properties and can be easily monitored using simple flow sensors. By monitoring the change in volume flow rate as a function of pneumatic actuation, we collocated sensing function with fluid transport in soft robotic systems, therefore creating new opportunities for the fabrication of autonomous, hybrid systems.

We measured the compressive stress–strain curve of PDMS (Figure S1, Supporting Information). The samples were prepared and tested according to the American Society for Testing of Materials (ASTM) standards for testing rubber and elastomeric materials (see Supporting Information).[30] We then used the stress–strain curve along with the second-order Ogden model to predict the deformation of our PDMS devices. The Ogden model was proposed to describe the stress–strain relationship of rubber-like hyperelastic materials. During a simple tension or compression experiment, the second-order Ogden model can be described as

$$\sigma = \sum_{i=1}^{2} \mu_i \left(\lambda^{\alpha_i - 1} - \lambda^{-\frac{\alpha_i}{2} - 1} \right) \quad (1)$$

where σ is the nominal stress, λ is the stretch ratio (can be given as $\varepsilon + 1$, where ε is strain), and μ_i ($\mu_1 = 0.301$ and $\mu_2 = 0.010$) and α_i ($\alpha_1 = -1.347$ and $\alpha_2 = -5.616$) are material constants, which were determined by fitting experimental data with the second-order Ogden model.

We simulated the CS geometry of the channel under compression using a mesh size of 100 μm. A fixed boundary condition was applied between the bottom of the PDMS device and the bottom plate. A contact boundary condition with friction coefficient (0.98)[31] was defined between the inner channel walls, and between the PDMS device surfaces (excluding the bottom surface) and the top/bottom plates (Figure 1a–d).

To validate these predictions experimentally, we fabricated a device with a straight rectangular channel of ≈35 mm length, and a cross section of 1.5 mm × 1.5 mm and measured the change in the channel morphology associated with varying amounts of compressive stress applied using a material testing system (Figure 1a–d). In particular, we measured (by observing the CS morphology of epoxy replicates as described earlier and in the Supporting Information) the geometric changes to the channel at specific displacement values, $\Delta d = d_i - d_f$, where d_i is the initial height of the device, and d_f is the final height (Figure 1e–g). The mechanical stress in these experiments ranged between 0 and 0.75 MPa. A PDMS device ($d_i = 8.8$ mm) was compressed by Δd values ranging between 0 and 1.6 mm corresponding to strain values ($\varepsilon = -\Delta d/d_i$) between 0 and −0.18 (Figure 1g, and Figure S3, Supporting Information). We used micro-CT to confirm that the channel deformed uniformly along its length (Figure 1f, and Figure S4, Supporting Information).

From these data, we determined that the CS morphology of the microchannels generated through simulation compared favorably with the experimentally determined CS areas (averaged from three cross sections) for different Δd values (Figure 1f). The CS area predicted by the model was similar (at 95% confidence) to the experimental values for Δd values ≤ 1.0 mm ($\varepsilon \geq -0.11$, Figure 1g). Beyond this value ($\Delta d > 1.0$ mm), the simulation failed to accurately capture the channel morphology. We attributed this variation (significantly different at 95% confidence) to the mismatch between measured stress–strain curves and the Ogden model in the nonlinear region (Figure S1, Supporting Information). The Ogden model fitted to the averaged measured stress–strain curves accurately predicted the elastomeric behavior within the linear region of the stress–strain curve, $-\varepsilon < 0.5$; however, it deviated with larger variations in the nonlinear region, $-\varepsilon > 0.5$ (Figure S1 and S5, Supporting Information).[22] The deviation between the results at $\Delta d > 1.0$ mm can be further explained by the fact that the maximum strain magnitude within the device for $\Delta d > 1.0$ mm reaches 0.5 (Figure S5, Supporting Information), which is indeed the value at which the Ogden model starts to deviate (Figure S1, Supporting Information). That said, the linear region is typically within the operational strain values of soft robots fabricated using elastomeric composites, and therefore, this limitation is not viewed as an impediment to the potential applications of the presented approach.[32]

While imaging of the replicates using optical microscopy or micro-CT was convenient, it was time-consuming and did not allow rapid surveying of the channel morphologies during continuous compression, i.e., when the devices are actively compressed to different stress states. We, therefore, developed an approach to observe the channel deformation in real time using an optical microscope attached to a material testing system (Figure S2, Supporting Information). This setup not only enabled rapid characterization of the channel deformation, but also allowed us to capture the deformation mechanics that were critical to define the boundary conditions for the FEM model (see Supporting Information and Video S1, Supporting Information).

We further expanded our investigation to devices with networks of channels (e.g., two and three channels in parallel) and studied their deformation for ε values ranging between 0 and −0.11 (**Figure 2**). The channels were symmetrically distributed within the device, and epoxy replicates were generated at six different Δd values (0, 0.2, 0.4, 0.6, 0.8, and 1.0 mm) with compressive stresses ranging from 0 to 0.35 MPa (Figure 2b,c,e,f, and Figure S6 and S7, Supporting Information). When compared, the CS areas of 10 out of 10 replicates for device with two channels and 11 out of 15 replicates for device with three channels were statistically indifferent from simulation at 95% confidence (Figure 2c,f). We point out that the simulation accurately predicted the final geometry, which was different depending on the location of the microchannel within the network. The knowledge gained through these investigations will be critical to understand different flow properties (for example, Reynolds number or Péclet number) that describe the degree of mixing or transport within the channels as a function of the channel CS morphology. The Reynolds number for the different channel morphologies ranged between 10 and 20, indicating laminar flow with low degrees of mixing, and the Péclet number ranged between 5000 and 10000 (see Supporting Information), suggesting mixing via advection. That said, the change in channel morphology will result in noticeably different flow velocity profiles and shear stress values within the different channels.

We used simulated channel dimensions to estimate the volume flow rate changes expected during the compression process (**Figure 3**a,c). For these calculations, we assumed Poiseuille flow through circular channels, because the exact solution for Poiseuille flow through the deformed channel geometries is not explicitly known, to estimate volume flow rates expected at various deformed states. For an undeformed circular channel,[33] the volume flow rate (Q) is given as

$$Q = \frac{\pi D^4}{128\mu}\left(\frac{\Delta p}{L}\right) \tag{2}$$

where D is the channel diameter, μ is the viscosity of fluid, Δp is the pressure difference between inlet and outlet of channel, and L is the length of the channel. For the deformed channels, we used hydraulic diameter ($D_h = 4A/P$, where $A =$ CS area and $P =$ wetted perimeter) instead of D. In these experiments, we can assume that L is constant and hold Δp constant throughout deformation, thus allowing Equation (2) to be simplified to $Q \propto {D_h}^4$. This simplification highlights the direct relationship between the hydraulic diameter of the channel and the volume flow rate, which states that at constant $\Delta p/L$, decreasing D_h (via compression) will necessarily require a decrease in the volume flow rate (Figure 3c). Based on these assumptions and an initial volume flow rate measured at $\Delta d = 0$ mm, we calculated the

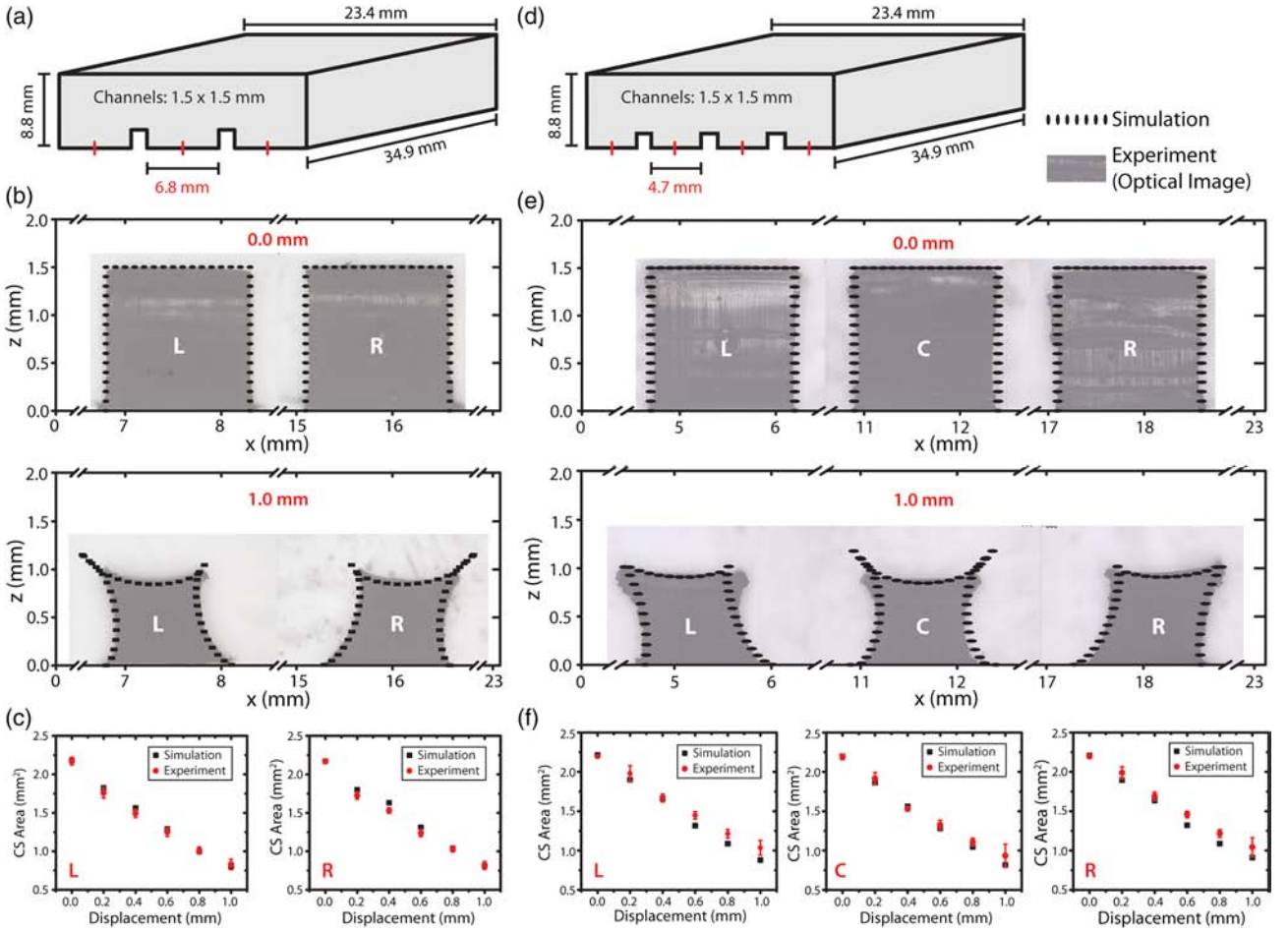

Figure 2. Deformation of multichannel devices. a,d) Schematics showing the dimensions and channel placement for a) two and d) three channels within the same microfluidic device. b,e) Optical micrographs of the channel replicates overlaid on the simulated profiles to compare the channel morphology (shown for Δd values of 0.0 and 1.0 mm). c,f) CS area comparison for c) two channels and f) three channels at displacements values of 0.0, 0.2, 0.4, 0.6, 0.8, and 1.0 mm. The left (L), center (C), and right (R) channels are annotated.

expected volume flow rate at different channel cross sections that were previously determined for different Δd values (0.15, 0.30, 0.45, 0.60, and 0.75 mm) (Figure 3c). These calculations indicate that a readily observable change in the flow rate (on the order of $\approx 30\,\mu L\,min^{-1}$) is expected to be associated with deformation of the microchannels to $-\varepsilon = \approx 0.09$.

To demonstrate the practical utility of this deformation-induced flow rate modulation, we designed a serpentine channel device with a rectangular cross section of 1.4 mm (h) × 0.7 mm (w) (Figure 3b) and experimentally measured the volume flow rates of liquids (pumped using a pneumatic flow system with Δp held constant) within the microchannels while they were actively deformed using a material testing system. We used discrete stress states, Δd values of 0, 0.15, 0.30, 0.45, 0.60, and 0.75 mm, which corresponded to stress values between 0 and 0.3 MPa (Figure 3d). As expected, at constant pressure, we observed a decrease in the volume flow rate as the channel was compressed. Moreover, the flow rates measured qualitatively agree with the simplified flow rate calculations described earlier (Figure 3c,d). The periodic peaks observed in the measured volume flow rates are due to sudden fluctuations in the pressure of the system as a result of the minor disturbances to the inlet/outlet ports of the devices during compression, which are difficult to eliminate completely. This idealized experiment sets the foundation for flow-based touch and bend sensing in soft robotics.

We used the deformation-modulated volume flow rate to sense touch or to detect the actuation state of a typical FEA. We fabricated the FEA following established protocols and attached a channel network to the top layer (Figure 3e).[1a] We then measured the change in the volume flow rate, at constant fluid pressure, to 1) sense touch (Figure 3f,h, plotted as a function of the force "f" applied) and 2) predict the actuation state of the robot (Figure 3g,i, and Video S2, Supporting Information). As expected from Equation (2), upon actuation, we observed a change in the volume flow rate in the top channel network. The actuation caused lateral expansion (increasing the width and decreasing the height of the cross section) of the channels while decreasing the hydraulic diameter, which would result in a lower volume flow rate (Figure 3c). This change in the volume

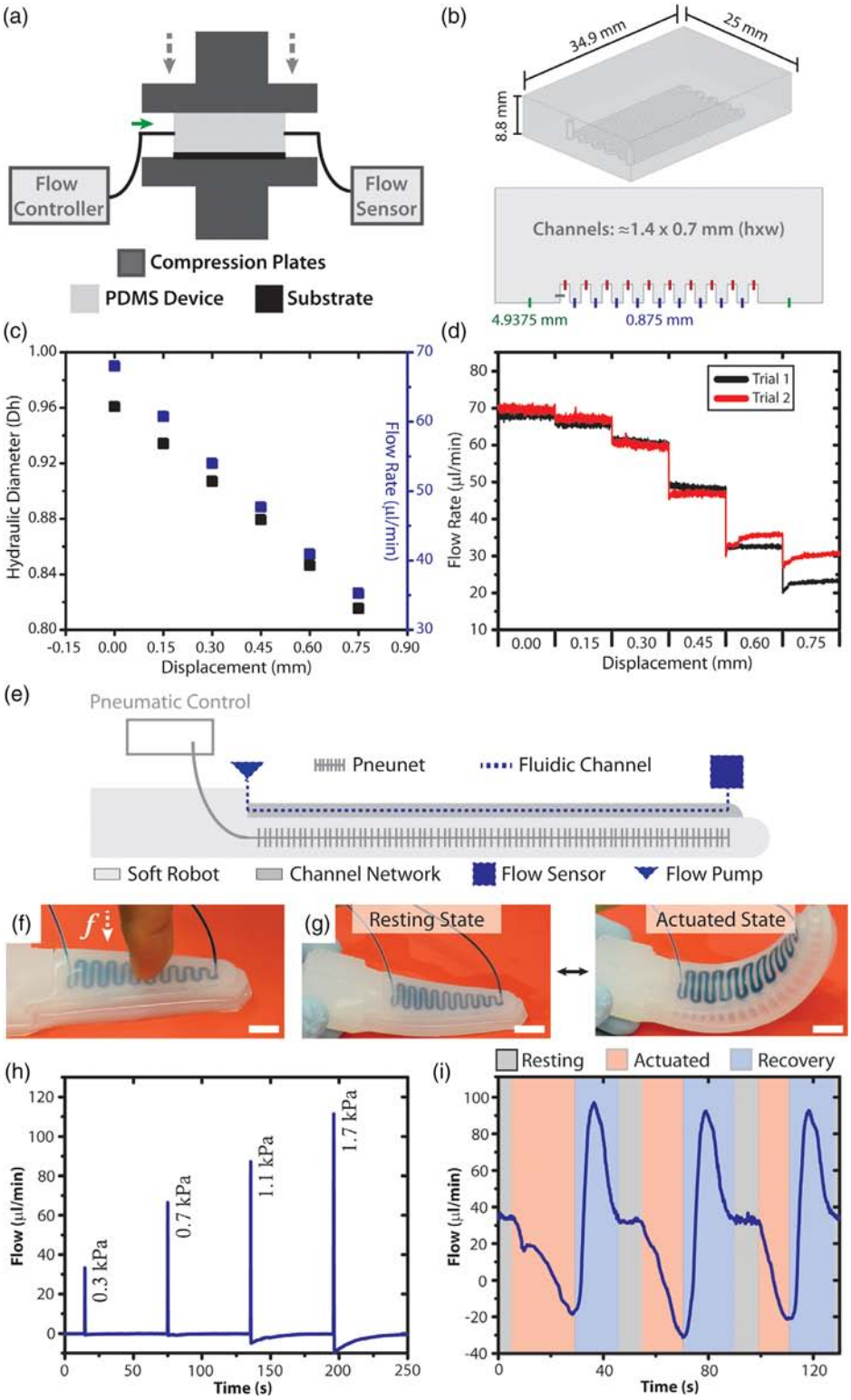

Figure 3. Touch and actuation sensing using deformable microchannels in soft robotic actuators. a) Schematic illustration of the testing system. b) Schematic of a device with a serpentine channel (critical dimensions are given). c) Plot showing the change in the hydraulic diameter (D_h) and the corresponding change in the flow rate as a function of displacement (Δd). d) Plot showing the change in the volume flow rate as a function of time at Δd values of 0, 0.15, 0.30, 0.45, 0.60, and 0.75 mm. e) Schematic of a soft robot with integrated channel networks on the top and bottom layers. f,g) Photographs of a soft robotic arm with microchannel network used to detect f) touch and g) actuation. Scale: 10 mm. h) Plot showing the change in the volume flow rate within the microchannel in response to touch, tested by applying varying amounts of force (0.3–1.7 kPa). i) Plot showing the change in the flow rate in response to actuation.

flow rate within the microchannels also enabled touch sensing following a similar logic (the force associated with touching the device decreased hydraulic diameter and thus volume flow rate). Volume flow rate through the microchannels was driven using a pneumatic control system set to operate at constant pressure. Any deformation of the network caused by touch or a change in the channel morphology and dimensions (as expected due to channel compression and extension during actuation) resulted in a necessary change in the flow rate through the device (indicated as maxima/minima in the flow rate traces, Figure 3h,i). In particular, a decrease in the flow rate was associated with a decrease in D_h during actuation ($Q \propto D_h^4$); the following increase in the flow rate is due to recovery of the pressure in the system when the actuator transitions back to a resting state (Figure 3i). We determined the limit of detection (minimum force required to observe a characteristic change in the flow rate) to be 75 Pa, and the response time to be between 50 and 100 ms, quantities that are comparable to existing sensors for soft actuators.[7c,f] Advanced soft robotic systems will require the transport of liquids for power generation, onboard diagnostics, and actuation—the use of flow dynamics within these systems for actuation and tactile sensing capabilities represents an opportunity in the collocation of multiple functionalities in soft robotic systems.

In conclusion, we demonstrated the ability to predict channel deformation (CS geometries and dimensions) using a finite-element model and experimentally verified this model using devices with single or multiple channels. In soft robotics, understanding the transport properties of various fluids (e.g., liquid metals, reagents, etc.) within the channels throughout the deformations associated with actuation will enable new design opportunities, such as hybrid systems with microchannel networks that colocalize multiple functions (e.g., fluid transport used for actuation, but also for sensing, detection, onboard analysis, etc.). The soft robotic systems demonstrated here, which provided simple, flow-based touch and actuation detection functionality, are the first to illustrate the capability of collocated liquid transport and sensing. Deformation-tunable soft channels could also influence several other fields, including the study of drug transport within the body (e.g., by mimicking the circulatory system) and molecular transport in microchannels.[11] Furthermore, the ability to reversibly control the channels could be useful to 1) analytical chemists for size-based particle separation; 2) forensic scientists for developing hand-operable, field deployable devices; 3) roboticists for building autonomous systems that collocate multiple functionalities; and 4) material scientists for developing stretchable/wearable microfluidic devices with potential applications in biomedicine, electronics, etc.

Supporting Information

Supporting Information is available from the Wiley Online Library or from the author.

Acknowledgements

A.K. and D.L. contributed equally to this work. The authors thank the Department of Chemistry and the Nebraska Center for Materials and Nano Science (NCMN), at the University of Nebraska–Lincoln for start-up funds. S.A.M. thanks 3M for support through a Non-Tenured Faculty Award. The authors thank Dr. Dong Wang (at UNMC) and Gang Zhao for their help and providing access to micro-CT instrument, and Dr. Mehrdad Negahban and Zesheng Zhang (at Department of Mechanical and Materials Engineering, UNL) for providing access to material testing system (MTS 810) used for mechanical studies. This research was performed in part at the NanoEngineering Research Core Facility, and at the Nebraska Nanoscale Facility: National Nanotechnology Coordinated Infrastructure and the Nebraska Center for Materials and Nanoscience, which are supported by the National Science Foundation under Award ECCS: 1542182, and the Nebraska Research Initiative.

Conflict of Interest

The authors declare no conflict of interest.

Keywords

microfluidics, soft actuators, soft lithography, soft robotics, tactile sensing

Received: May 21, 2019
Revised: June 13, 2019
Published online: July 19, 2019

[1] a) R. F. Shepherd, F. Ilievski, W. Choi, S. A. Morin, A. A. Stokes, A. D. Mazzeo, X. Chen, M. Wang, G. M. Whitesides, *Proc. Natl. Acad. Sci. USA* **2011**, *108*, 20400; b) M. Wehner, R. L. Truby, D. J. Fitzgerald, B. Mosadegh, G. M. Whitesides, J. A. Lewis, R. J. Wood, *Nature* **2016**, *536*, 451.

[2] a) W. J. Lan, E. J. Maxwell, C. Parolo, D. K. Bwambok, A. B. Subramaniam, G. M. Whitesides, *Lab Chip* **2013**, *13*, 4103; b) A. Rana, Y. Zhang, L. Esfandiari, *Analyst* **2018**, *143*, 2971.

[3] a) K. S. Elvira, X. Casadevall i Solvas, R. C. Wootton, A. J. deMello, *Nat. Chem.* **2013**, *5*, 905; b) T. Schneider, J. Kreutz, D. T. Chiu, *Anal. Chem.* **2013**, *85*, 3476; c) E. K. Sackmann, A. L. Fulton, D. J. Beebe, *Nature* **2014**, *507*, 181; d) A. Konda, S. A. Morin, *Nanoscale* **2017**, *9*, 8393; e) Y. Liu, X. Jiang, *Lab Chip* **2017**, *17*, 3960; f) A. Konda, A. Rau, M. A. Stoller, J. M. Taylor, A. Salam, G. A. Pribil, C. Argyropoulos, S. A. Morin, *Adv. Funct. Mater.* **2018**, *28*, 1803020.

[4] a) S. Y. Teh, R. Lin, L. H. Hung, A. P. Lee, *Lab Chip* **2008**, *8*, 198; b) X. Fan, I. M. White, *Nat. Photonics* **2011**, *5*, 591.

[5] B. Mosadegh, P. Polygerinos, C. Keplinger, S. Wennstedt, R. F. Shepherd, U. Gupta, J. Shim, K. Bertoldi, C. J. Walsh, G. M. Whitesides, *Adv. Funct. Mater.* **2014**, *24*, 2163.

[6] a) D. Huh, K. L. Mills, X. Zhu, M. A. Burns, M. D. Thouless, S. Takayama, *Nat. Mater.* **2007**, *6*, 424; b) S. M. Park, Y. S. Huh, H. G. Craighead, D. Erickson, *Proc. Natl. Acad. Sci. U. S. A.* **2009**, *106*, 15549; c) D. Tepáyotl-Ramírez, T. Lu, Y.-L. Park, C. Majidi, *Appl. Phys. Lett.* **2013**, *102*, 044102.

[7] a) C. Majidi, R. Kramer, R. J. Wood, *Smart Mater. Struct.* **2011**, *20*, 105017; b) J. T. B. Overvelde, Y. Mengüç, P. Polygerinos, Y. Wang, Z. Wang, C. J. Walsh, R. J. Wood, K. Bertoldi, *Extreme Mech. Lett.* **2014**, *1*, 42; c) R. A. Bilodeau, E. L. White, R. K. Kramer, in *IEEE/RSJ Int. Conf. on Intelligent Robots and Systems*, IEEE, Hamburg, Germany **2015**; d) J. C. Yeo, H. K. Yap, W. Xi, Z. Wang, C.-H. Yeow, C. T. Lim, *Adv. Mater. Technol.* **2016**, *1*, 1600018; e) E. L. White, J. C. Case, R. K. Kramer, *Sens. Actuators, A.* **2017**, *253*, 188; f) K. Elgeneidy, N. Lohse, M. Jackson, *Mechatronics* **2018**, *50*, 234.

[8] a) C. Dagdeviren, P. Joe, O. L. Tuzman, K.-I. Park, K. J. Lee, Y. Shi, Y. Huang, J. A. Rogers, *Extreme Mech. Lett.* **2016**, *9*, 269; b) J. Shintake, E. Piskarev, S. H. Jeong, D. Floreano, *Adv. Mater. Technol.* **2018**, *3*, 1700284; c) M. Maselli, D. Zrinscak, V. Magliola, M. Cianchetti, in *2nd IEEE Int. Conf. on Soft Robotics*, IEEE, Seoul, Korea **2019**; d) M. T. Chorsi, E. J. Curry, H. T. Chorsi, R. Das, J. Baroody, P. K. Purohit, H. Ilies, T. D. Nguyen, *Adv. Mater.* **2019**, *31*, 1802084.

[9] a) R. F. Shepherd, A. A. Stokes, J. Freake, J. Barber, P. W. Snyder, A. D. Mazzeo, L. Cademartiri, S. A. Morin, G. M. Whitesides, *Angew. Chem., Int. Ed.* **2013**, *52*, 2892; b) P. Polygerinos, N. Correll, S. A. Morin, B. Mosadegh, C. D. Onal, K. Petersen, M. Cianchetti, M. T. Tolley, R. F. Shepherd, *Adv. Eng. Mater.* **2017**, *19*, 1700016; c) S. I. Rich, R. J. Wood, C. Majidi, *Nat. Elec.* **2018**, *1*, 102.

[10] a) S. H. Song, C. K. Lee, T. J. Kim, I. C. Shin, S. C. Jun, H. I. Jung, *Microfluid. Nanofluid.* **2010**, *9*, 533; b) M. E. Wilson, N. Kota, Y. Kim, Y. D. Wang, D. B. Stolz, P. R. LeDuc, O. B. Ozdoganlar, *Lab Chip* **2011**, *11*, 1550; c) G. Guan, L. Wu, A. A. Bhagat, Z. Li, P. C. Chen, S. Chao, C. J. Ong, J. Han, *Sci. Rep.* **2013**, *3*, 1475.

[11] A. O. Bicen, I. F. Akyildiz, in *IEEE Int. Conf. on Communications Workshops*, IEEE, Budapest, Hungary **2013**.

[12] Y. Hallez, J. Magnaudet, *Phys. Fluids* **2008**, *20*, 053306.

[13] a) A. Skardal, T. Shupe, A. Atala, *Drug Discovery Today* **2016**, *21*, 1399; b) Y. S. Zhang, J. Aleman, S. R. Shin, T. Kilic, D. Kim, S. A. Mousavi Shaegh, S. Massa, R. Riahi, S. Chae, N. Hu, H. Avci, W. Zhang, A. Silvestri, A. Sanati Nezhad, A. Manbohi, F. De Ferrari, A. Polini, G. Calzone, N. Shaikh, P. Alerasool, E. Budina, J. Kang, N. Bhise, J. Ribas, A. Pourmand, A. Skardal, T. Shupe, C. E. Bishop, M. R. Dokmeci, A. Atala, A. Khademhosseini, *Proc. Natl. Acad. Sci. USA* **2017**, *114*, E2293.

[14] S. A. Morin, R. F. Shepherd, S. W. Kwok, A. A. Stokes, A. Nemiroski, G. M. Whitesides, *Science* **2012**, *337*, 828.

[15] a) R. L. Truby, M. Wehner, A. K. Grosskopf, D. M. Vogt, S. G. M. Uzel, R. J. Wood, J. A. Lewis, *Adv. Mater.* **2018**, *30*, e1706383; b) A. Koivikko, E. S. Raei, M. Mosallaei, M. Mäntysalo, V. Sariola, *IEEE Sens. J.* **2018**, *18*, 223.

[16] T. Shay, O. D. Velev, M. D. Dickey, *Soft Matter* **2018**, *14*, 3296.

[17] W. Zhou, Y. Huang, E. Menard, N. R. Aluru, J. A. Rogers, A. G. Alleyne, *Appl. Phys. Lett.* **2005**, *87*, 251925.

[18] C. Zhao, X. Xu, Q. Yang, T. Man, S. J. Jonas, J. J. Schwartz, A. M. Andrews, P. S. Weiss, *Nano Lett.* **2017**, *17*, 5035.

[19] a) P. Moseley, J. M. Florez, H. A. Sonar, G. Agarwal, W. Curtin, J. Paik, *Adv. Eng. Mater.* **2016**, *18*, 978; b) M. F. Roslan, N. M. Shaffiar, M. K. N. Khairusshima, I. S. S. Sharifah, *IOP Conf. Ser.: Mater. Sci. Eng.* **2018**, *290*, 012022; c) D. Lee, A. Erickson, T. You, A. T. Dudley, S. Ryu, *Lab Chip* **2018**, *18*, 2077.

[20] I. D. Johnston, D. K. McCluskey, C. K. L. Tan, M. C. Tracey, *J. Micromech. Microeng.* **2014**, *24*, 035017.

[21] a) T. K. Kim, J. K. Kim, O. C. Jeong, *Microelectron. Eng.* **2011**, *88*, 1982; b) L. C. S. Nunes, *Mater. Sci. Eng., A* **2011**, *528*, 1799.

[22] R. W. Ogden, *Proc. R. Soc. London, Ser. A* **1972**, *326*, 565.

[23] R. S. Rivlin, D. W. Saunders, *Philos. Trans. R. Soc., A* **1948**, *241*, 379.

[24] O. H. Yeoh, *Rubber Chem. Technol.* **1993**, *66*, 754.

[25] M. Mooney, *J. Appl. Phys.* **1940**, *11*, 582.

[26] A. Konda, J. M. Taylor, M. A. Stoller, S. A. Morin, *Lab Chip* **2015**, *15*, 2009.

[27] J. C. McDonald, M. L. Chabinyc, S. J. Metallo, J. R. Anderson, A. D. Stroock, G. M. Whitesides, *Anal. Chem.* **2002**, *74*, 1537.

[28] J. C. Case, E. L. White, R. K. Kramer, *Soft Robot.* **2015**, *2*, 80.

[29] D. L. Logan, *A First Course in the Finite Element Method*, Cengage Learning, Boston, MA, USA **2011**.

[30] ASTM, Standard Test Methods for Rubber Property-Compression Set, **2014**.

[31] K. Chawla, S. Lee, B. P. Lee, J. L. Dalsin, P. B. Messersmith, N. D. Spencer, *J. Biomed. Mater. Res., Part A* **2009**, *90*, 742.

[32] R. V. Martinez, A. C. Glavan, C. Keplinger, A. I. Oyetibo, G. M. Whitesides, *Adv. Funct. Mater.* **2014**, *24*, 3003.

[33] F. M. White, in *Fluid Mechanics* (Ed: F. M. White), McGraw-Hill, New York **2017**, p. 347.